applied sciences

MDPI

Article

Evolution of a Geothermal System with Fluid Re-Injection

Angiolo Farina [1], Antonio Fasano [2,3], Mario Primicerio [1,3] and Fabio Rosso [1,*]

[1] Dipartimento di Matematica e Informatica "U. Dini", University of Firenze, 50134 Firenze, Italy; angiolo.farina@unifi.it (A.F.); mario.primicerio@gmail.com (M.P.)
[2] FIAB SpA, Vicchio, 50039 Firenze, Italy; a.fasano@fiab.it
[3] I.A.C.–C.N.R., Via dei Taurini, 00185 Roma, Italy
* Correspondence: fabio.rosso@unifi.it; Tel.: +39-055-4237434

Received: 21 September 2020; Accepted: 21 October 2020; Published: 27 October 2020



Abstract: In this paper, we study the stationary configurations of a vapor-dominated geothermal system. We propose a general mathematical model, which turns out to be a free boundary problem, and we focus on the stationary solutions. The analysis, developed considering the data of the geothermal field in Larderello, Tuscany (Italy), shows that steady-stable states may exist both when the re-injection takes place in depth and when the natural recharge is distributed both in the area occupied by vapor and in the one occupied by liquid.

Keywords: geothermal system; flow in porous media; steady state

1. Introduction

In volcanic areas, geothermal energy represents an important resource. For instance, the Tuscan basins of Larderello and Monte Amiata provide almost 30% of the energetic need of the whole region (see, for example, [1,2]). Several studies have been devoted to geothermal reservoirs with the aim of providing mathematical models—some of them very sophisticated—for extraction wells [3–10]. Here we refer to a specific situation—a vapor-dominated system [11,12]—in which the reservoir is sealed at the top by a nearly impermeable rock layer, under which water is in the vapor state up to a depth at which the pressure and temperature are such that it is present as liquid. Wells are drilled through the impermeable layer to reach the high-pressure vapor zone. The vapor then leaves the reservoir, and extraction is sustained by the vaporization of deep water (sometimes called plutonic or juvenile water). This is the case for the Larderello geothermal system (one of the largest in the world), which is characterized by a reservoir pressure that is much lower than hydrostatic pressure. This is a consequence of its natural evolution from an initial liquid-dominated to the current vapor-dominated system [3,10].

The genesis of vapor-dominated reservoirs has intrigued researchers for many years. In 1973, Truesdell and White [6] reviewed all the principal conceptual models proposed until then for the reservoir and possible mechanisms for superheating the steam. These models aimed to give a qualitative description of the physical processes leading to the development of a vapor-dominated reservoir. However, all efforts notwithstanding, many open questions remain.

A reservoir is always formed by a complex of fractured permeable rocks confined between impermeable layers and saturated by water, in a liquid and/or vapor phase. As far as the Larderello geothermal field is concerned, the heat source is a magmatic intrusion located at a relatively small depth (5–10 km) producing temperatures of $500 \div 700$ °C in the rocks surrounding the reservoir. Both the lower and upper boundaries of the reservoir depend on the local lithology. The so-called K horizon (a seismic reflecting surface), strictly related to a temperature of about 450 °C, is considered

to represent the bottom of the geothermal reservoir [10,13,14]. The top of the productive reservoir is set in correspondence to the first fractured level in the central areas of the field, where a great amount of well data are available. In the peripheral areas, where well data are lacking, the top is set in correspondence to the 250 °C isotherm [13–16]. Usually, the shallow carbonate–anhydrite reservoir shows a temperature of 220 ÷ 250 °C and pressure of about 15 ÷ 20 bar at 1000 m depth, while the deep metamorphic reservoir has a temperature of 300 ÷ 350 °C and pressure around 70 bar at 3000 m depth [13].

The sustainable management of geothermal resources basically involves setting up and maintaining a specific long-term production scheme [17,18]. It also involves the basic ingredients of successful geothermal resource management; i.e., re-injection, monitoring and modeling [14,19,20]. However, the term "sustainable development" has many other important implications and has received ever-increasing attention over the last decade or two [21–29].

Vapor-dominated geothermal fields are still little understood, and their production histories are so short that premonitory indications of exhaustion are not yet generally recognized. In the 1970s, Sestini [30] concluded that the production of steam from the Larderello fields at that time was approaching a steady state and could have been maintained for many years. However, Truesdell and White [6] came to quite different conclusions, saying that the Larderello field was approaching exhaustion. This appears to have been sustained 30 years later, as the time series of production shows, in the papers by Romagnoli et al. [10] and Barelli [9]. In this context, the study of water levels reported in 1978 by Celati et al. [31] is of great importance.

In the last 20 years, due to the increase of the power demand from renewable sources, many studies have investigated the Larderello–Travale geothermal field using fully three-dimensional models [10,14,32–34]. Clearly, the reliability of the forthcoming conclusions of these approaches depends heavily upon the reliability of the boundary and initial conditions selected. In general, these studies are validated against the current rates of production with the aim of predicting future scenarios.

The present contribution focuses on the modeling of geothermal systems in which extraction, natural and artificial recharge mechanisms may act simultaneously. Indeed, the extracted geothermal fluid, after its utilization in a power plant, can be injected back into the reservoir through specific injection wells. For instance, in Larderello, re-injection activities started in the 1970s to contrast the production decline [2,13]. In this way, the natural recharge of the reservoir (by meteoric or juvenile water) is artificially integrated, drastically reducing the impact on the environment of power-plant operations [35,36].

The aim of this study is to investigate the existence and stability of possible equilibrium configurations that can guarantee sustainable production. We develop a model that is able to give some basic information. Of course, approximations have been introduced in order to develop a model which is mathematically treatable. For example, the fluid in the reservoir is assumed to be pure water; this is a very schematic description, as, in practice, many chemicals are carried by the water, which makes the real thermodynamics much more complex. Next, we consider a region with a cluster of wells distributed so that the vapor motion underneath can be reasonably considered to be one-dimensional. This may appear to be an excessive approximation, but actually it is largely justified by the fact that problems such as this are characterized by a great level of data uncertainty. Our model is a one-dimensional parabolic free boundary problem, where both extraction and recharge are treated as source terms in the continuity equation. In this framework, we develop a model describing the behavior of the geothermal field, the location of the water vaporization front and its stability with respect to perturbations. More precisely, we examine the steady (or quasi-steady) state attained by recharging the reservoir with water, looking for those recharging rates compatible with a stable state. In particular, we discuss the effects of both extraction and recharge (both natural and artificial). We determine the steady solution by solving a non-linear equation which, when peculiar conditions are met, has more than a single solution. A linear stability analysis of the stationary liquid/vapor

interface (if it exists) is then used to select the physically acceptable solution. In particular, we show that selecting the parameters according to the field data allows us to obtain a stable interface that is qualitatively in agreement with the borehole extraction/injection data. In this respect, our model, although extremely simple, allows us to obtain some insights regarding the state of the reservoir and to predict the location of the phase transition surface. On one hand, the simplicity of the model has the advantage that one can deal with an exact solution; on the other hand, the price to pay is that a classical validation remains questionable,as a sharp liquid/vapor interface is very unlike to exist in a real field. However, it should also be taken into account that that even highly sophisticated three-dimensional models depend significantly upon the boundary and initial conditions imposed. In the majority of cases (and for Larderello in particular), these conditions suffer from a great degree of uncertainty that greatly influences the reliability of the model predictions.

The paper continues as follows. Section 2 is devoted to the general 1D model. The analysis of the stationary solutions is illustrated in Sections 3 and 4. In Section 5, we relate the results to some historical field data for a better interpretation and justification of the model. The conclusions are drawn in the last section.

2. The Mathematical Model

We consider a geothermal fluid composed of water in a gaseous and liquid state. We denote by x the vertical axis pointing upward. The bottom and the top of the geothermal reservoir correspond to $x = L_i$ $(L_i < 0)$ and to $x = L_s$ $(L_s < 0)$, respectively. The ground surface corresponds to $x = 0$, so that the domain of interest is $[L_i, L_s]$. We assume that the width of the capillary fringe is negligible with respect to the vertical dimensions of the reservoir, and thus that there is a clear separation between the liquid and the vapor phase through a sharp interface, $x = s(t)$, that may vary in time. So, the lower part of the domain $L_i \leq x \leq s(t)$, is saturated with liquid, while in the upper part of the domain, $s(t) \leq x \leq L_s$, there is only vapor. At $x = L_s$ the vapor pressure is known, and we denote it as P_s. The latter is a measured datum and essentially depends on the exploitation of the basin.

In Table 1, we list the values of the constants involved in the model. These parameters are compatible with those available for some areas of the geothermal field of Larderello, Tuscany [10,14].

Table 1. List of parameters referring to the reservoir of Larderello [10,14]. All dimensionless constants used in the present work are evaluated by using these values. A full list of additional simbols is reported in Table 3.

Symbol	Description	Value	Units
L_s	Reservoir top depth	-1000	m
L_i	Reservoir bottom depth	-3500	m
T_s	Temperature at the top of the reservoir	550	K
γ	Thermal gradient	0.04	K/m
P_s	Vapor pressure at the top of the reservoir	9×10^5	Pa
r	Universal gas constant over H_2O molar mass	4.6×10^2	J/(kg K)
ρ_l	Liquid water density (at local conditions)	$\approx 8 \times 10^2$	kg/m^3
ϕ	Medium porosity	2×10^{-2}	-
g	Standard gravity	9.8	m/s^2
μ	Vapor viscosity	2×10^{-5}	Pa s
κ	Medium permeability	$\approx 5 \times 10^{-15}$	m^2
K_T	Thermal conductivity	≈ 2	W/(m K)

According to the experimental data [37–39], the temperature within the reservoir is linear:

$$T(x) = T_s + \gamma (L_s - x), \quad L_i \leq x \leq L_s, \tag{1}$$

where $\gamma > 0$, constant in time, is the known thermal gradient (see Table 1). We also set

$$L = L_s - L_i (= 2500\,\mathrm{m})\,. \tag{2}$$

Remark 1. *The given value of γ in Table 1 implies that the temperature at depth $L_i = -3500\,\mathrm{m}$ is 650 K. Assuming a surface temperature of 300 K, we have a geothermal gradient in the caprock of $\gamma_{cap} = 0.25\,\mathrm{K/m}$. This may be surprising, since this value is about three times the value commonly indicated in textbooks as the typical gradient in a geothermal field (generally $0.08\,\mathrm{K/m}$) and actually requires that the average thermal conductivity of the caprock be rather low—say $0.32\,\mathrm{W/(mK)}$. A simple explanation is that the mean gradient of the field is indeed based upon the estimated depth of the K horizon (in the present case, around $-5000\,\mathrm{m}$) and the isotherm which identifies the K horizon itself (about 750 K), leading, correctly, to $\gamma_{mean} = 0.08\,\mathrm{K/m}$. On the other hand, the question is much more complex. In a very recently published article [39], the great variability of the thermal conductivity K_T of rocks at Larderello and their strong dependence on temperature and, to a much lesser extent, on pressure were clearly emphasized. Reported values vary from less that $2\,\mathrm{W/(mK)}$ to more then $4.5\,\mathrm{W/(mK)}$ depending on the core sample depth and exploration well. Furthermore, the evaluated geothermal gradient has a great variability with depth, reaching values, for some layers, close to $\gamma_{cap} = 0.2\,\mathrm{K/m}$—not far from the value proposed in Table 1.*

The domain $s(t) \leq x \leq L_s$ is saturated by vapor whose continuity equation is

$$\frac{\partial}{\partial t}(\phi\rho) + \frac{\partial}{\partial x}(\phi\rho v) = \phi d_v, \qquad s(t) < x \leq L_s, \tag{3}$$

where $\phi(x)$ is medium porosity (see Table 1), v is the velocity of the vapor, ρ is its density and d_v is the vapor source/sink density rate (with dimensions $\mathrm{kg\,m^{-3}s^{-1}}$). In general, d_v is due to both the recharge vapor (generated from the vaporization of meteoric recharge water), which mixes with the vapor inside the reservoir, and the extraction/re-injection due to external devices [40]. In general, the rate d_v depends on the local pressure, or rather on the difference between the external pressure and the local pressure. More specifically, we split d_v into two contributions: a recharge generated from the vaporization of recharge water (which may depend on the local pressure) and a point-wise recharge due to N injection/extraction wells whose extraction/injection rates depend on the difference between the local pressure and the re-injection pressure:

$$d_v = d_{v,\mathrm{met}}(P) + \sum_{i=1}^{N} d_{v,\mathrm{inj}}^{(i)} J_v^{(i)} \left(P - P_{\mathrm{inj}}^{(i)}\right) \delta(x - x_i)\,, \tag{4}$$

where the subscripts "met" and "inj" mean, respectively, "of meteoric origin" and "due to injection", P denotes the vapor pressure, δ denotes the Dirac delta, x_i is the location of the ith injection head, $d_{v,\mathrm{inj}}^{(i)}$ is the order of magnitude of the density rate, where $J_v^{(i)}$ (dimensionless) gives its dependence on the pressure difference, and $P_{\mathrm{inj}}^{(i)}$ is the injection pressure.

The vapor is assumed to behave as a perfect gas; i.e.,

$$\rho = \frac{P}{rT}, \tag{5}$$

where r is the molar vapor constant (see Table 1). Using the generalized Darcy's law [41],

$$\phi v = -\frac{\kappa}{\mu(P,T)}\left(\frac{\partial P}{\partial x} + \rho g\right), \tag{6}$$

where μ is the vapor viscosity, which depends on both temperature and pressure, and $\kappa(x)$ is the permeability of the medium (see again Table 1), ρ is as in Equation (5) and g is the gravity acceleration; thus, we rewrite (3) as

$$\frac{1}{T}\frac{\partial P}{\partial t} - \frac{1}{\phi(x)}\frac{\partial}{\partial x}\left[\frac{\kappa(x)\ P}{\mu(P,T)\ T}\left(\frac{\partial P}{\partial x} + \frac{g}{r}\frac{P}{T}\right)\right] = r d_v(P), \qquad s(t) < x \leq L_s < 0, \tag{7}$$

where T is given by (1).

In the liquid region $L_i \leq x \leq s(t)$, the continuity equation is written as

$$\frac{\partial \phi \rho_\ell}{\partial t} + \frac{\partial}{\partial x}(\phi \rho_\ell v_\ell) = \rho_\ell \phi d_\ell, \qquad L_i \leq x \leq s(t), \tag{8}$$

where ρ_ℓ is the density of the liquid, v_ℓ is the liquid velocity and d_ℓ is the liquid water source density rate (with a dimension of s^{-1}), due to both re-injection and natural recharge fluid. The solution to Equation (8) is

$$v_\ell(x,t) = \frac{1}{\phi(x)\rho_\ell(T,P)}\int_{L_i}^{x} \phi(\xi)\left(d_\ell \rho_\ell - \frac{\partial \rho_\ell}{\partial t}\right) d\xi, \qquad L_i < x < s(t) \leq L_s < 0, \tag{9}$$

where, for simplicity, we have neglected $v_\ell(L_i,t)$, and where the pressure P is the hydrostatic pressure.

The continuity of the mass flux across $s(t)$ implies that $\rho v - \rho_\ell v_\ell = -\dot{s}(\rho_\ell - \rho)$ [42]. As $\rho \ll \rho_\ell$, we can approximate this relation with

$$\dot{s} = \left(1 + \frac{\rho}{\rho_\ell}\right) v_\ell - \frac{\rho}{\rho_\ell} v. \tag{10}$$

Thus, recalling Equations (6) and (9), we obtain

$$\dot{s} = D_\ell \left(1 + \frac{P}{\rho_\ell r T}\right)_{x=s(t)} + \left[\frac{P}{rT\rho_\ell}\frac{\kappa}{\phi\mu}\left(\frac{\partial P}{\partial x} + \frac{P}{rT}g\right)\right]_{x=s(t)}, \tag{11}$$

where

$$D_\ell = \frac{1}{(\phi\rho_\ell)_{x=s(t)}}\int_{L_i}^{s(t)} \phi(\xi)\left(d_\ell \rho_\ell - \frac{\partial \rho_\ell}{\partial t}\right) d\xi, \tag{12}$$

which (with a dimension of $\mathrm{m\,s}^{-1}$) is the total recharge rate in the liquid domain. In particular, we assume that we can identify two distinct effects:

(i) Recharge due to the meteoric waters, denoted by $d_{\ell,\mathrm{met}}$, which, as $d_{v,\mathrm{met}}$, may depend on the local pressure;
(ii) Recharge due to clusters of re-injection wells which, for simplicity, we assume to be concentrated in M locations.

Thus, setting

$$d_\ell(x) = \underbrace{d_{\ell,\mathrm{met}}}_{\substack{\text{meteoric}\\ \text{recharge}}} + \underbrace{\sum_{i=i}^{M} d_{\ell,\mathrm{inj}}^{(i)} J_\ell^{(i)}\left(P(x_i) - P_{\mathrm{inj}}^{(i)}\right)\delta(x - x_i)}_{\text{re-injection}}, \tag{13}$$

where, as in (4), the injection rates depend on the difference between the re-injection pressure P_{inj} and the local pressure. Indeed, $d_{\ell,\mathrm{inj}}^{(i)}$, $i = 1, 2, \ldots, M$, gives the injection rate order of magnitude,

while $J_\ell^{(i)}\left(P\left(x_i\right)-P_{\text{inj}}^{(i)}\right)$, which is dimensionless, gives the dependence on the pressure difference. We thus have

$$\begin{aligned} D_\ell &= \frac{\int_{L_i}^{s(t)} \phi(\xi)\left[\left(d_{\ell,\text{met}}+\sum_{i=i}^{M} d_{\ell,\text{inj}}^{(i)}\mathcal{L}_\ell^{(i)}(\xi)\right)\rho_\ell-\frac{\partial \rho_\ell}{\partial t}\right]d\xi}{\phi\left(s\left(t\right)\right)\ \rho_\ell\left(T,P\right)|_{s(t)}} \\ &= \frac{d_{\ell,\text{met}}\int_{L_i}^{s(t)} \phi\left(\xi\right)\left[\left(1+\sum_{i=i}^{M}\frac{d_{\ell,\text{inj}}^{(i)}}{d_{\ell,\text{met}}}\mathcal{L}_\ell^{(i)}(\xi)\right)\rho_\ell\left(P,T\right)-\frac{\partial \rho_\ell\left(P,T\right)}{\partial t}\right]d\xi}{\phi\left(s\left(t\right)\right)\ \rho_\ell\left(T,P\right)|_{s(t)}}. \end{aligned}$$

where

$$\mathcal{L}_\ell^{(i)}(x)=J_\ell^{(i)}\left(P\left(x\right)-P_{\text{inj}}^{(i)}\right)\delta\left(x-x_i\right) \tag{14}$$

A second free boundary condition is provided by Clapeyron's law, which gives the relationship between P and T at the liquid/vapor interface. In the range of temperature relevant to our problem, this law takes the following empirical form:

$$P^*=a\exp\left[b\frac{T-273}{T}\right], \tag{15}$$

where T is in Kelvin, P in Pascal and a and b have values of $a=9.617\times10^2$ Pa, $b=17.35$. Consequently, the second condition on the free boundary is

$$P\left(s\left(t\right),t\right)=P^*\left(T\left(s\left(t\right)\right)\right), \tag{16}$$

and (11) rewrites as

$$\begin{aligned} \dot{s} &= D_\ell\left[1+\frac{P^*}{rT\rho_\ell}\right]_{x=s(t)} \\ &+ \left[\frac{P^*}{rT\rho_\ell}\frac{\kappa}{\phi\mu}\left(\frac{\partial P}{\partial x}+\frac{P^*}{rT}g\right)\right]_{x=s(t)}. \end{aligned} \tag{17}$$

We remark that (16) requires the following condition be fulfilled:

$$P\left(x,t\right)<P^*\left(T\left(x\right)\right), \text{in the vapor domain; i.e., } s(t)<x\leq L_s, \tag{18}$$

in order to obtain a physically consistent solution.

To complete the information, we need to give the pressure at the reservoir top, $P\left(L_s,t\right)=P_s$ (see Table 1) and the initial conditions $s\left(0\right)=s_o$, $L_i<s_o<L_s$, $P\left(x,0\right)=P_o\left(x\right)$, $s_o<x<L_s$, fulfilling Equations (18) and (16); i.e., $P_o\left(x\right)<P^*\left(T\left(x\right)\right)$ and $P_o\left(s_o\right)=P^*\left(T\left(s_o\right)\right)$.

Thus, the mathematical problem to be solved is the following: find a time $\tau>0$, a function $s\left(t\right)\in C\left[0,\tau\right]\cap C^1\left(0,\tau\right)$ such that $s\left(t\right)\in\left(L_i,L_s\right)$ and a function $P\left(x,t\right)\in C^{2,1}\left(D_\tau\right)$, continuous in

$\overline{D}_\tau = \{(x,t) \mid s(t) \le x \le L_s,\ 0 \le t \le \tau\}$, where $\partial_x P$ is continuous up to $x = s(t)$, $t \in (0,\tau)$, so that, for $T(x)$ given by Equation (1), the following system is fulfilled:

$$\begin{cases} \dfrac{\partial P}{\partial t} - \dfrac{T}{\phi}\dfrac{\partial}{\partial x}\left[\dfrac{\kappa P}{T\,\mu}\left(\dfrac{\partial P}{\partial x} + \dfrac{g}{r}\dfrac{P}{T}\right)\right] = rTd_v(P), \qquad (x,t) \in D_\tau, \\ P(L_s,t) = P_s, \qquad t \in [0,\tau], \\ P(s(t),t) = P^*(T(s(t))), \qquad t \in [0,\tau], \\ \dot{s} = D_\ell \left[1 + \dfrac{P^*}{rT\rho_\ell}\right]_{x=s(t)} \\ \quad + \left[\dfrac{P^*}{rT\rho_\ell}\dfrac{\kappa}{\phi\mu}\left(\dfrac{\partial P}{\partial x} + \dfrac{P^*}{rT}g\right)\right]_{x=s(t)}, \quad t \in (0,\tau), \\ P(x,0) = P_o(x), \qquad x \in [s_o, L_s], \\ s(0) = s_o, \qquad s_o \in (L_i, L_s), \end{cases} \tag{19}$$

According to the results in [43,44], the problem has one unique solution provided that $P_o \in C[s_o, L_s]$.

3. Steady-State Solutions

We consider a steady state (meaning that neither d_v nor d_ℓ depend on time) and normalize space, temperature and pressure in the following way:

$$\widetilde{x} = \frac{x - L_s}{L}, \ \Leftrightarrow \ \widetilde{x} \in [-1,0], \qquad \widetilde{s} = \frac{s - L_s}{L}, \ \Leftrightarrow \ \widetilde{s} \in [-1,0], \tag{20}$$

$$\widetilde{T} = \frac{T}{T_s}, \qquad \widetilde{P} = \frac{P}{P_c},$$

where P_c is a characteristic pressure, which still needs to be selected. Recalling Equation (1), we consider $\widetilde{T}$ to be an independent variable; namely

$$\widetilde{T} = 1 - \widetilde{\Gamma}\,\widetilde{x}, \quad \Longleftrightarrow \quad \widetilde{T} \in \left(1, 1 + \widetilde{\Gamma}\right), \tag{21}$$

where

$$\widetilde{\Gamma} = \frac{\gamma L}{T_s} \approx 0.18\,.$$

We remark that, because of the change of the variable in Equation (20), $\widetilde{T} = 1$ corresponds to the top of the basin while $1 + \widetilde{\Gamma}$ to the bottom.

Next, we introduce

$$\widetilde{\sigma}(t) = \left.\widetilde{T}\right|_{\widetilde{x}=\widetilde{s}(t)}, \tag{22}$$

as the temperature at the interface, so that

$$\widetilde{\sigma} = 1 - \widetilde{\Gamma}\,\widetilde{s}\,, \quad \Longleftrightarrow \quad \widetilde{\sigma} \in \left(1, 1 + \widetilde{\Gamma}\right). \tag{23}$$

Then, we set

$$f(\widetilde{\sigma}) = \widetilde{P}^*(\widetilde{\sigma}) = \frac{a}{P_c}\exp\left[b\frac{\widetilde{\sigma} - 273/T_s}{\widetilde{\sigma}}\right]. \tag{24}$$

We also set $\rho_\ell\left(\widetilde{T}\right)=\rho_{\ell,o}\widetilde{\rho}_\ell\left(\widetilde{T}\right)$, $\mu\left(\widetilde{P},\widetilde{T}\right)=\mu_o\widetilde{\mu}\left(\widetilde{P},\widetilde{T}\right)$, $\kappa\left(\widetilde{T}\right)=\kappa_o\widetilde{\kappa}\left(\widetilde{T}\right)$, with $\widetilde{\mu}$, $\widetilde{\rho}_\ell$ and $\widetilde{\kappa}$ being dimensionless; $\phi\left(\widetilde{T}\right)=\phi_o\widetilde{\phi}\left(\widetilde{T}\right)$, with ϕ_o giving the porosity order of magnitude, so that

$$\frac{P^*\left(T\left(s(t)\right)\right)}{rT\left(s(t)\right)\rho_\ell\left(P^*,T\left(s(t)\right)\right)}=\left(\frac{P_c}{rT_s\rho_{\ell,o}}\right)h\left(\widetilde{\sigma}\right),\quad\text{with}\quad h\left(\widetilde{\sigma}\right)=\frac{f\left(\widetilde{\sigma}\right)}{\widetilde{\sigma}\,\widetilde{\rho}_\ell\left(\widetilde{\sigma}\right)},\tag{25}$$

and

$$D_\ell=\frac{d_{\ell,\text{met}}\,T_s}{\gamma}\,\widetilde{D}_\ell,\tag{26}$$

with

$$\widetilde{D}_\ell=\frac{1}{\phi\left(\widetilde{\sigma}\right)\,\rho_\ell\left(\widetilde{\sigma},f\left(\widetilde{\sigma}\right)\right)}\int_{\widetilde{\sigma}}^{1+\widetilde{\Gamma}}\left[1+\sum_{i=i}^{M}\mathfrak{R}_\ell^{(i)}\mathcal{L}_\ell^{(i)}\left(\widetilde{P}\right)\right]\rho_\ell\left(\widetilde{P},\widetilde{T}\right)\phi\left(\widetilde{T}\right)\,d\widetilde{T},\tag{27}$$

where $\mathcal{L}_\ell^{(i)}$ has been defined in Equation (14) and

$$\mathfrak{R}_\ell^{(i)}=\frac{d_{\ell,\text{inj}}^{(i)}}{d_{\ell,\text{met}}}.\tag{28}$$

Setting $P_c=P_s$, the steady dimensionless version of problem (19), 1, (19), 2, and (19), 3 is

$$\begin{cases}\dfrac{1}{\phi\left(T\right)}\dfrac{\partial}{\partial T}\left[\dfrac{\kappa\left(T\right)}{\mu\left(P,T\right)}\dfrac{P}{T}\left(\dfrac{\partial P}{\partial T}-\eta\dfrac{P}{T}\right)\right]=-\beta_v\left(T,P\right),\qquad 1<T<\sigma,\\[2ex] P(1)=1,\\[2ex] P(\sigma)=f(\sigma),\end{cases}\tag{29}$$

where $\eta=\dfrac{g}{r\gamma}\approx 0.533$, $f(\sigma)$ is given by Equation (24) and

$$\beta_v\left(P,T\right)=\left(\frac{\phi_o}{\kappa_o}\frac{r\,\mu_o T_s^3}{\gamma^2P_s^2}\,d_{v,\text{met}}\right)\left[1+\sum_{i=1}^{N}\mathfrak{R}_v^{(i)}J_v^{(i)}\left(P-P_{\text{inj}}^{(i)}\right)\delta\left(T-T_i\right)\right],\tag{30}$$

and

$$\mathfrak{R}_v^{(i)}=\frac{d_{v,\text{inj}}^{(i)}}{d_{v,\text{met}}},\qquad i=1,2,\ ...,\ N.\tag{31}$$

Here and in the following, we omit the "~" to keep the notation as clear as possible.

The steady (dimensionless) version of (19), 4 is

$$F\left(\sigma\right)=0,\tag{32}$$

where

$$\begin{aligned}F\left(\sigma\right)\;&=\left(\frac{d_{\ell,\text{met}}\,T_s}{\gamma}\right)\,D_\ell\left[1+\left(\frac{P_s}{rT_s\rho_{\ell,o}}\right)h\left(\sigma\right)\right]\\&+\left(\frac{\kappa_oP_s^2\,\gamma}{\phi_o\,r\rho_{\ell,o}\mu_o\,T_s^2}\right)\,\frac{\kappa\left(\sigma\right)\,h\left(\sigma\right)}{\phi\left(\sigma\right)\,\mu\left(f\left(\sigma\right),\sigma\right)}\Omega\left(\sigma\right),\end{aligned}\tag{33}$$

with

$$\Omega\left(\sigma\right)=\eta\frac{f\left(\sigma\right)}{\sigma}-\left.\frac{\partial P}{\partial T}\right|_\sigma.\tag{34}$$

In Section 4, we see that the set of steady solutions (Equation (32)) depends upon a set of n suitable parameters $\zeta_1, \ldots \zeta_n$. Thus, Equation (32) writes, more precisely,

$$F(\sigma; \zeta_1, \ldots, \zeta_n) = 0, \tag{35}$$

where $\zeta_1 and \ldots \zeta_n$ are dimensionless. Our approach consists first of verifying that $F = 0$ can be made explicit, under some limitations, with respect to a specific parameter—say ζ_1—that is

$$\zeta_1 = \mathfrak{F}(\sigma, \zeta_2, \ldots, \zeta_n). \tag{36}$$

Then, we look for the existence of stable, steady solutions to the system (Equations (29) and (32)) by varying the other parameters. Thus, for a given steady state σ_{st}, the study of its stability to small perturbations is reduced to investigate the following:

$$\frac{\partial F}{\partial \sigma}\left(\sigma_{st}, \mathfrak{F}\left(\sigma_{st}, \zeta_2, \ldots, \zeta_n\right), \zeta_2, \ldots, \zeta_n\right). \tag{37}$$

4. Numerical Simulations

In this section, we analyze some specific cases which represent some of the most significant physical situations. For the sake of simplicity, we take $\widetilde{\rho}_\ell\left(\widetilde{T}\right) = \mu\left(\widetilde{P}, \widetilde{T}\right) = \widetilde{\kappa}\left(\widetilde{T}\right) = \phi\left(\widetilde{T}\right) = 1$, so that h, given by Equation (25), simplifies to $h(\sigma) = f(\sigma)/\sigma$. Next, we assume that the injection rate is independent of the difference between the injection pressure and local pressure, and therefore $J_\alpha\left(P - P_{\text{inj}}^{(i)}\right) = 1, \alpha = v, \ell$.

There are many cases, and it is impossible to analyze them all. We therefore focus on these issues:

1. Recharge due to both liquid groundwater and to vapor injection in the vapor domain;
2. Recharge due to groundwater occurring in the whole domain (liquid and vapor) and to vapor extraction/injection localized in the vapor domain;
3. Artificial recharge due to liquid injection localized in the liquid domain.

To see the explicit form of Equation (36), it is more convenient to proceed by subsequent steps.

Suppose, for a moment, that $\beta_v = 0$. This will help us to understand (and also visualize graphically) the effect of $\beta_v \neq 0$.

Proposition 1. *For $\beta_v = 0$, Equation (33) can be written in the form*

$$\omega_2 = \mathfrak{F}_0(\sigma), \tag{38}$$

and has a maximum in $(\sigma_o, \omega_{2,o}) \approx \left(1.066, 1.29 \times 10^{-6}\right)$.

Proof. The solution to (29) is

$$P^2(T, \sigma) = T^{2\eta} - A(\sigma)\left(T^{2\eta} - T^2\right), \quad 1 \leq T \leq \sigma, \tag{39}$$

where

$$A(\sigma) = \frac{f^2(\sigma) - \sigma^{2\eta}}{\sigma^2 - \sigma^{2\eta}}. \tag{40}$$

In this case,

$$\left.\frac{\partial P}{\partial T}\right|_\sigma = \frac{1}{\sqrt{f(\sigma)}}\left[\eta\sigma^{2\eta-1} + A(\sigma)\left(\sigma - \eta\sigma^{2\eta-1}\right)\right], \tag{41}$$

so that $\Omega(\sigma) = \Omega_1(\sigma)$, with

$$\Omega_1(\sigma) = \eta\frac{f(\sigma)}{\sigma} - \frac{1}{\sqrt{f(\sigma)}}\left[\eta\sigma^{2\eta-1} + A(\sigma)\left(\sigma - \eta\sigma^{2\eta-1}\right)\right]. \tag{42}$$

Next, assuming that the liquid recharge occurs only in a part of the domain, D_ℓ given by (27) becomes

$$D_\ell = 1 + \Gamma - T_1\,, \tag{43}$$

for some (given) $T_1 < 1 + \Gamma$ and F, as defined by Equation (33), can be rewritten as

$$F(\sigma) = (1 + \Gamma - T_1)\left(1 + \omega_1\frac{f(\sigma)}{\sigma}\right) + \omega_2\frac{f(\sigma)}{\sigma}\Omega(\sigma)\,, \tag{44}$$

with

$$\omega_1 = \frac{P_s}{rT_s\rho_{\ell,o}}, \quad \omega_2 = \frac{\kappa_o P_s^2\,\gamma^2}{\phi_o\, r\rho_{\ell,o}\mu_o\, T_s^3 d_{\ell,\mathrm{met}}}, \tag{45}$$

and Ω is given by Equation (42). Clearly, Equation (44) is meaningful only for $1 < \sigma < T_1 < 1 + \Gamma$, showing that T_1 remains in the liquid domain. Function Ω_1 monotonically increases and is negative in $(1, 1 + \Gamma)$. Therefore, we have $-\infty < \Omega_1(\sigma) \le \Omega_1(1 + \Gamma) < 0$, meaning that we can express $F|_{\beta_v=0} = 0$ in the form of Equation (38). With the values in Table 1, the function $\mathfrak{F}_o$ has a maximum value in $(\sigma_o, \omega_{2,o}) \approx (1.066, 1.29 \times 10^{-6})$. □

Remark 2. *The physical situation corresponding to Equation (38) is a limit case in which the reservoir receives mass only in the liquid layer. This does not seem to be the case for Larderello, where the vapor region is also fed by steam of meteoric origin, as reported by many authors [40,45]. However, the artificial re-injection of geothermal wastewater is practiced in many geothermal fields as a means for reservoir pressure support and cannot be ignored [46–48]. We consider these more significant situations in the following three subsections.*

4.1. Case 1. Recharge Due to Liquid Groundwater Recharge and a Single Vapor Extraction/Injection Well

We now prove that, also in this case, the equation $F = 0$ can be solved explicitly as in Equation (38) provided that the injection rate and the well depth fulfill suitable conditions.

In this case, D_ℓ is still given by Equation (43) while $d_v = d_{v,\mathrm{inj}}\delta(x - x_o)$. Thus, β_v given by (30) becomes a constant

$$\beta_v(P, T) = \hat{\beta}_v, \quad \text{with} \quad \hat{\beta}_v = \frac{\phi_o}{\kappa_o}\frac{r\,\mu_o T_s^3}{\gamma^2 P_s^2}\, d_{v,\mathrm{inj}}\,. \tag{46}$$

Integrating Equation (29), 1 once, we obtain

$$\frac{P}{T}\left(\frac{\partial P}{\partial T} - \eta\frac{P}{T}\right) = -\hat{\beta}_v\theta(T - T_o) + C_1\,, \tag{47}$$

where C_1 is an integration constant, θ is the Heaviside function and T_o is the injection well depth. Setting $z = P^2/2$, Equation (47) becomes

$$z' - 2\eta\frac{z}{T} = C_1 T - \hat{\beta}_v T\theta(T - T_o)\,,$$

whose general solution is

$$z(T) = C_2 T^{2\eta} - \frac{C_1 T^2}{2(\eta - 1)} - \frac{\hat{\beta}_v}{2(\eta - 1)}\left[T^{2\eta}\int_1^T \tau^{2-2\eta}\delta(\tau - T_o)\,d\tau - T^2\theta(T - T_o)\right],$$

where $\theta(T - T_o)$ is the Heaviside function. By imposing boundary conditions (29), 2, and (29), 3, we get

$$\begin{aligned} P^2(T) &= \underbrace{T^{2\eta} - A(\sigma)\left(T^{2\eta} - T^2\right)}_{\text{for } \hat{\beta}_v = 0} + \underbrace{\frac{\hat{\beta}_v}{\eta - 1}\left[\left(\frac{\sigma^{2\eta} T_o^{2-2\eta} - \sigma^2}{\sigma^{2\eta} - \sigma^2}\right)\left(T^{2\eta} - T^2\right)\right.}_{\text{additional term for } \hat{\beta}_v \neq 0} \\ &- \underbrace{\left. T^{2\eta}\int_1^T \tau^{2-2\eta}\delta(\tau - T_o)\,d\tau + T^2\theta(T - T_o)\right]}_{\text{additional term for } \hat{\beta}_v \neq 0}, \end{aligned} \tag{48}$$

with $A(\sigma)$ given by Equation (40), which reduces to Equation (39) when $\hat{\beta}_v = 0$. In particular,

$$\begin{aligned} \left.\frac{\partial P}{\partial T}\right|_\sigma &= \frac{1}{\sqrt{f(\sigma)}}\left[\eta\sigma^{2\eta-1} + A(\sigma)\left(\sigma - \eta\sigma^{2\eta-1}\right)\right] \\ &+ \frac{\hat{\beta}_v}{(\eta - 1)\sqrt{f(\sigma)}}\left[\frac{\sigma^{2\eta} T_o^{2-2\eta} - \sigma^2}{\sigma^{2\eta} - \sigma^2}\left(\eta\sigma^{2\eta-1} - \sigma\right) - \left(\eta\sigma^{2\eta-1} T_o^{2-2\eta} - \sigma\right)\right], \end{aligned} \tag{49}$$

so that $\left.\frac{\partial P}{\partial T}\right|_\sigma$ tends to (41) when $\hat{\beta}_v \to 0$ and when $T_o \to 1$ (as physically expected).

To prove that the equation $F = 0$ can be solved explicitly, notice first that, because of (49), Ω has a different form, namely

$$\Omega = \Omega_1(\sigma) + \hat{\beta}_v \mathcal{G}(\sigma, T_o), \tag{50}$$

where Ω_1 is given by Equation (42) and

$$\mathcal{G}(\sigma, T_o) = \frac{\left[\frac{\sigma^{2\eta} T_o^{2-2\eta} - \sigma^2}{\sigma^{2\eta} - \sigma^2}\left(\eta\sigma^{2\eta-1} - \sigma\right) - \left(\eta\sigma^{2\eta-1} T_o^{2-2\eta} - \sigma\right)\right]}{(\eta - 1) f(\sigma)}. \tag{51}$$

To use the explicit form in Equation (36), we need $\Omega(\sigma, T_o) \neq 0$. It is convenient now to fix an upper limit to the variability of T_o—say $\mathfrak{T}_o$. Then, it can be seen that

$$\mathcal{G}(\sigma, \mathfrak{T}_o) < \mathcal{G}(\sigma, T_o) < 0, \qquad \forall T_o \in (1, \mathfrak{T}_o).$$

As a consequence, condition $\Omega \neq 0$ is fulfilled provided the variability of $\hat{\beta}_v$ is bounded below, namely

$$\hat{\beta}_v > \hat{\beta}_{v,\mathrm{cr}}(\mathfrak{T}_o) = -\frac{|\Omega_1(1 + \Gamma)|}{|\mathcal{G}(1 + \Gamma, \mathfrak{T}_o)|}. \tag{52}$$

Remark 3. *The critical value* (52) *tends to* $-\infty$ *for* $\mathfrak{T}_o$ *going to 1. Thus, we always consider only values of* T_o *close to but distinct from 1. We notice also that we have to take care of this lower bound only when we consider the case of extraction; that is,* $\hat{\beta}_v < 0$*. For example, for* $T_o = 1.0005$*, we are allowed to consider only* $\hat{\beta}_v \gtrsim -2.98 \times 10^6$*. On the other hand, from the physical point of view, negative values of* ω_2*, which show natural liquid recharge, are meaningless. Thus, recalling* (44)*, physically meaningful solutions to Equation* (35) *exist if and only if* Ω *remains negative. For example, for* $T_o = 1.0005$ *and* $\sigma \in (T_o, 1 + \Gamma)$*, the negativity of Equation* (50) *holds true provided that* $\hat{\beta}_v \gtrsim -1.13 \times 10^5$*.*

In the present case, steady states are described by

$$\omega_2 = \mathfrak{F}_1(\sigma, T_o, \hat{\beta}_v),$$

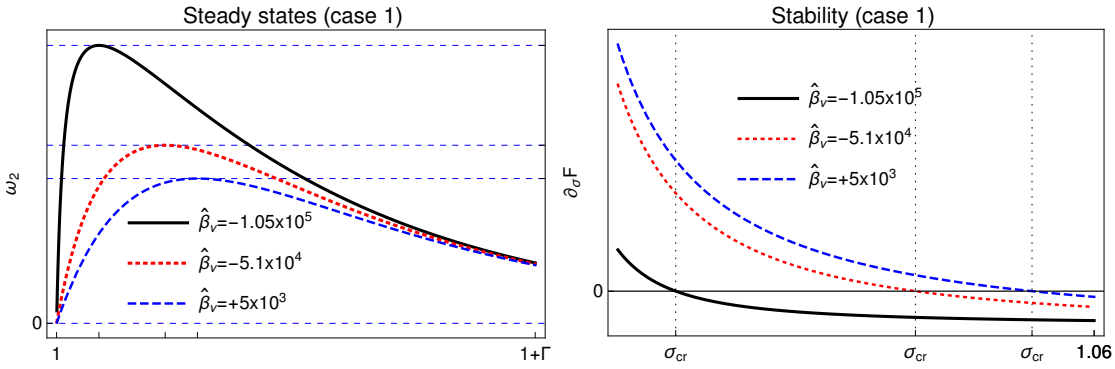
where

$$\mathfrak{F}_1 = -\left(\Omega(\sigma, T_o)\frac{f(\sigma)}{\sigma}\right)^{-1}(1+\Gamma-T_1)\left(1+\omega_1\frac{f(\sigma)}{\sigma}\right),$$

and Ω is given by Equation (50). Recalling Equation (37), we need to study the sign of

$$\frac{\partial F}{\partial \sigma}(\sigma, \mathfrak{F}_1(\sigma, T_o, \hat{\beta}_v)),$$

by varying both $T_o \in (1, \mathfrak{T}(\sigma))$ and $\hat{\beta}_v$. Figure 1 provides a synthetic picture of the varying influence of $\hat{\beta}_v$ in determining stable/unstable states.



(**a**) $T_o = 1.0005$, $T_1 = 1.07$. (**b**) Stability intervals.

Figure 1. (a) Steady states for $\hat{\beta}_v < 0$ when $T_o = 1.0005$ and $T_1 = 1.06$. (b) The critical values are $\sigma_{cr,1} \approx 1.016$, $\omega_{cr,1} \approx 7.7 \times 10^{-5}$ for $\hat{\beta}_v = -1.05 \times 10^5$, $\sigma_{cr,2} \approx 1.041$, $\omega_{cr,2} \approx 4.9 \times 10^{-5}$ for $\hat{\beta}_v = -5.1 \times 10^4$, and $\sigma_{cr,2} \approx 1.053$, $\omega_{cr,2} \approx 4 \times 10^{-5}$ for $\hat{\beta}_v = +5 \times 10^3$: all steady states for $\sigma > \sigma_{cr}$ and $\omega_2 < \omega_{cr}$ are stable in both cases. In dimensional variables, these values correspond, respectively, to the interfaces located at -1221 m, -1567 m and -1735. The liquid recharge occurs in a liquid layer that is 1675 m thick. The well-bore bottom hole is placed at -1007 m.

We have (linearly) stable steady solutions only for $0 < \omega_2 \leq \omega_{2,cr}$ and $\sigma \geq \sigma_{cr}$. Figure 1 shows that by decreasing $\hat{\beta}_v$ from positive values (injection) to negative ones (extraction), $\omega_{2,cr}$ increases and σ_{cr} decreases (i.e., the physical free boundary shifts towards the top of the reservoir). This means that the liquid region increases due to the augmented meteoric liquid recharge, as physically expected. Figure 2 shows that solutions represented in Figure 1 satisfy the compatibility condition (18).

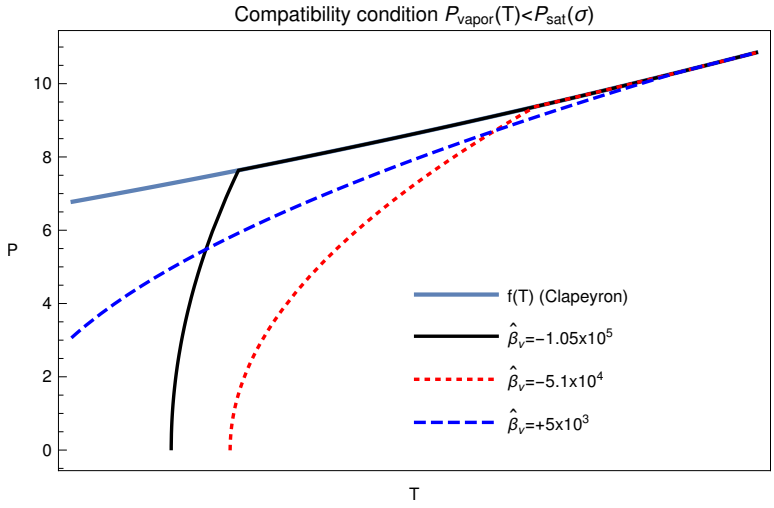


Figure 2. Check of the compatibility condition (18) for case 1.

4.2. Case 2. Groundwater Recharge Occurring in the Whole Domain and a Single Vapor Extraction/Injection Well

The procedure to obtain the explicit form of $F = 0$ is similar to that in Section 4.1, but function Ω is more complex. Calculations are presented in such a way to emphasize the differences with respect to Section 4.1.

In this case $\mathfrak{R}_\ell^{(i)} = 0$, D_ℓ is given by $1 + \Gamma - \sigma$ (since $T_1 = \sigma$), and β_v, given by (30), has the form

$$\beta_v(P,T) = B_v\left[1 + \mathfrak{R}_v\delta(T - T_o)\right], \quad \text{with} \quad B_v = \frac{\phi_o}{\kappa_o}\frac{r\,\mu_o T_s^3}{\gamma^2 P_s^2}\, d_{v,\text{met}}\ . \tag{53}$$

Therefore, Equation (29), 1 becomes

$$\frac{\partial}{\partial T}\left[\frac{P}{T}\left(\frac{\partial P}{\partial T} - \eta\frac{P}{T}\right)\right] = -B_v\left[1 + \mathfrak{R}_v\delta(T - T_o)\right].$$

Since $B_v\mathfrak{R}_v = \hat{\beta}_v$, after one integration, we obtain

$$\frac{P}{T}\left(\frac{\partial P}{\partial T} - \eta\frac{P}{T}\right) = -\hat{\beta}_v\theta(T - T_o) - B_v T + C_1\ ,$$

where C_1 is the integration constant. Setting again $z = P^2/2$, we get

$$z' - 2\eta\frac{z}{T} = C_1 T - \hat{\beta}_v T\theta(T - T_o) - B_v T^2,$$

whose general solution is

$$z(P) = \underbrace{C_2 T^{2\eta} - \frac{C_1 T^2}{2(\eta - 1)} - \frac{\hat{\beta}_v}{2(\eta - 1)}\left[T^{2\eta}\int_1^T \tau^{2-2\eta}\delta(\tau - T_o)\,d\tau - T^2\theta(T - T_o)\right]}_{\text{case 1}} + \underbrace{\frac{B_v T^3}{2(\eta - 3/2)}}_{\text{additional term}},$$

where C_2 is the second integration constant. Proceeding as in Section 4.1 (i.e., imposing the boundary conditions in Equations (29), 2, and (29), 3) we obtain

$$P^2(T) = \underbrace{T^{2\eta} - A(\sigma)\left(T^{2\eta} - T^2\right) + \frac{\hat{\beta}_v}{\eta - 1}\left[\left(\frac{\sigma^{2\eta}T_o^{2-2\eta} - \sigma^2}{\sigma^{2\eta} - \sigma^2}\right)\left(T^{2\eta} - T^2\right)\right.}_{\text{case 1}}$$
$$\underbrace{\left. - T^{2\eta}\int_1^T \tau^{2-2\eta}\delta(\tau - T_o)\,d\tau + T^2\theta(T - T_o)\right]}_{\text{case 1}}$$
$$\underbrace{+\frac{B_v}{\eta - 3/2}\left[T^3 - T^{2\eta} - \left(\frac{\sigma^3 - \sigma^{2\eta}}{\sigma^{2\eta} - \sigma^2}\right)\left(T^{2\eta} - T^2\right)\right]}_{\text{additional term}},$$

where $A(\sigma)$ is given by Equation (40), which reduces to Equation (48) when $B_v = 0$ and to Equation (39) when $\hat{\beta}_v = 0$. Next,

$$\begin{aligned}\left.\frac{\partial P}{\partial T}\right|_{\sigma} &= \frac{1}{\sqrt{f(\sigma)}}\left[\eta\sigma^{2\eta-1} + A(\sigma)\left(\sigma - \eta\sigma^{2\eta-1}\right)\right] \\ &+ \frac{\hat{\beta}_v}{(\eta-1)\sqrt{f(\sigma)}}\left[\frac{\sigma^{2\eta}T_o^{2-2\eta} - \sigma^2}{\sigma^{2\eta} - \sigma^2}\left(\eta\sigma^{2\eta-1} - \sigma\right) - \left(\eta\sigma^{2\eta-1}T_o^{2-2\eta} - \sigma\right)\right] \\ &+ \frac{B_v}{(\eta-3/2)\sqrt{f(\sigma)}}\left[\frac{3}{2}\sigma^2 - \eta\sigma^{2\eta-1} + \left(\frac{\sigma^3 - \sigma^{2\eta}}{\sigma^{2\eta} - \sigma^2}\right)\left(\sigma - \eta\sigma^{2\eta-1}\right)\right],\end{aligned}$$

which gives (49) when $B_v = 0$. Thus, recalling Equations (34), (42) and (50), we have

$$\Omega = \Omega_1(\sigma) + \hat{\beta}_v \mathcal{G}(\sigma, T_o) + B_v \mathcal{H}(\sigma),$$

where

$$\mathcal{H}(\sigma) = \frac{1}{(\eta-3/2)\sqrt{f(\sigma)}}\left[\frac{3}{2}\sigma^2 - \eta\sigma^{2\eta-1} + \left(\frac{\sigma^3 - \sigma^{2\eta}}{\sigma^{2\eta} - \sigma^2}\right)\left(\sigma - \eta\sigma^{2\eta-1}\right)\right].$$

Function H monotonically decreases and is negative. Therefore, $0 > \mathcal{H}(\sigma) > \mathcal{H}(1+\Gamma) \approx -0.015$.

Remark 4. *Recalling what we emphasized in Remark 3, in order to obtain physically meaningful solutions to Equation (38), we need Ω to remain negative when we change $\hat{\beta}_v$ and B_v. For fixed $T_o \in (1, \mathfrak{T}_o)$ and $\hat{\beta}_v > \beta_{cr}(\mathfrak{T}_o)$; this implies*

$$B_v > B_{v,cr}(\sigma, \hat{\beta}_v, \mathfrak{T}_o) = -\frac{\Omega_1(\sigma) + \hat{\beta}_v \mathcal{G}(\sigma, \mathfrak{T}_o)}{\mathcal{H}(\sigma)}. \tag{54}$$

Figure 3 shows the level lines (the white boxes indicate some values) of $B_{v,cr}$ for all $\sigma \in (1, 1+\Gamma)$ and $\hat{\beta}_v$ varying over 10 orders of magnitude from negative to positive values, when $\mathfrak{T}_o = 1.0005$. To handle a specific case, one fixes $\hat{\beta}_v > \beta_{cr}(\mathfrak{T}_o)$ and uses $\sup_{\sigma > T_o} B_{cr}(\sigma, \hat{\beta}_v, \mathfrak{T}_o)$ as a critical value. We notice that only non-negative values of B_v, which is the meteoric recharge, are of physical interest; when $\hat{\beta}_v \geq 0$, $\sup_{\sigma > T_o} B_{v,cr}$ is negative ($\approx -1.9 \times 10^4$) and Equation (54) does not need to be invoked. For $\hat{\beta}_v$ negative (extraction), $\sup_{\sigma > T_o} B_{v,cr}$ continues to be negative as long as $\hat{\beta}_v > -1.13 \times 10^5$. Thus in our simulations, we always keep $\hat{\beta}_v \geq -10^5$.

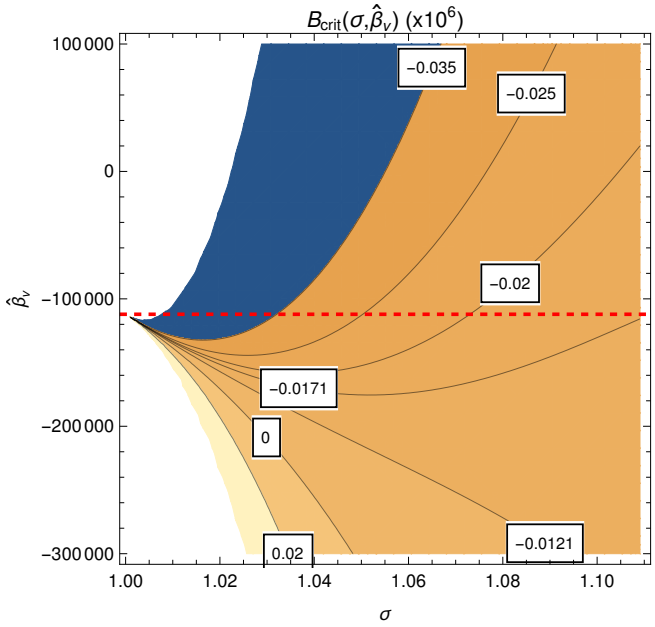
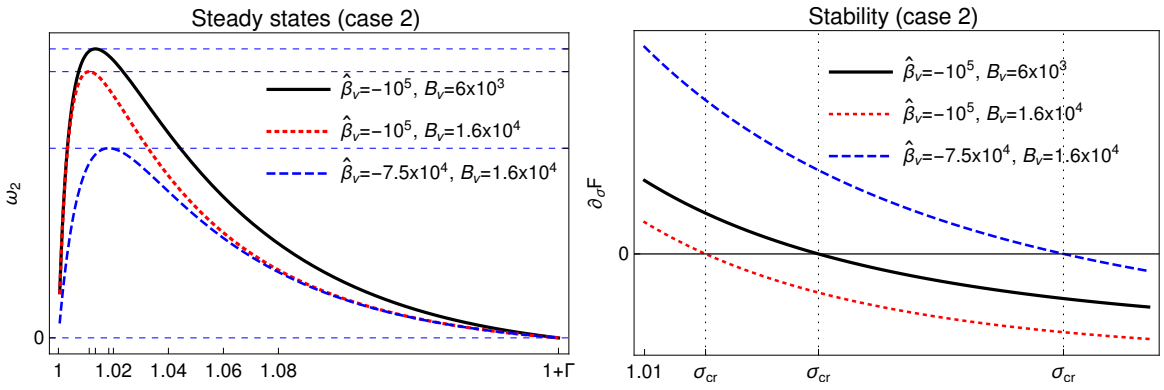


Figure 3. Some level lines $B_{\rm cr}(\sigma,\hat{\beta}_v)$=const. for $\mathfrak{T}_o = 1.0005$ (the white boxes indicate the value of the constant). The grid-line $\hat{\beta}_v = -1.13 \times 10^5$ (in red) shows that, for $\hat{\beta}_v > -1.13 \times 10^5$, B_v is negative for all $\sigma \in (T_o, 1+\Gamma)$.



(**a**) $B_v > 0$, $\hat{\beta}_v < 0$. (**b**) Stability intervals.

Figure 4. (**a**) Steady statesfor $T_o = 1.0005$, two negative values of $\hat{\beta}_v$ and two positive values of B_v. (**b**) For $\hat{\beta}_v = -10^5$ and $B_v = 10^5$, the critical values $\sigma_{\rm cr}$ and $\omega_{\rm cr}$ are, respectively, ≈1.01345 and $\approx 9 \times 10^{-5}$. For $\hat{\beta}_v = - \times 10^5$ and $B_v = 1.6 \times 10^4$, the critical values $\sigma_{\rm cr}$ and $\omega_{\rm cr}$ are, respectively, ≈1.011 and $\approx 8.3 \times 10^{-5}$. For $\hat{\beta}_v = -7.5 \times 10^4$ and $B_v = 1.6 \times 10^4$, the critical values $\sigma_{\rm cr}$ and $\omega_{\rm cr}$ are, respectively, ≈1.018 and 6×10^{-5}. All steady states for $\sigma > \sigma_{\rm cr}$ and $\omega_2 < \omega_{2,\rm cr}$ are stable. In dimensional variables, these values correspond, respectively, to the critical interface being located at −1185 m, −1154 m and −1252 m.

We have stable steady solutions only for $0 < \omega_2 \leq \omega_{2,\rm cr}$ and $\sigma \geq \sigma_{\rm cr}$. Figure 4 shows that by increasing $\hat{\beta}_v$ and keeping $B_v > 0$ fixed, $\omega_{2,\rm cr}$ decreases while $\sigma_{\rm cr}$ increases. On the contrary, increasing B_v and keeping $\hat{\beta}_v < 0$ fixed causes $\omega_{2,\rm cr}$ to decrease and $\sigma_{\rm cr}$ to decrease. This behavior also agrees with physical expectations. Indeed, increasing the vapor extraction with a fixed vapor recharge (i.e., from the blue curve to the red one) implies that $\sigma_{\rm cr}$ decreases, and the liquid natural recharge needs to be adjusted at higher rates to maintain stability. On the other hand, a fixed extraction rate and a decreasing natural vapor recharge (i.e., from the red curve to the black one) imply that, to maintain stability, the liquid natural recharge must increase and the critical interface must increase. Figure 5 shows that the compatibility condition (18) is satisfied.

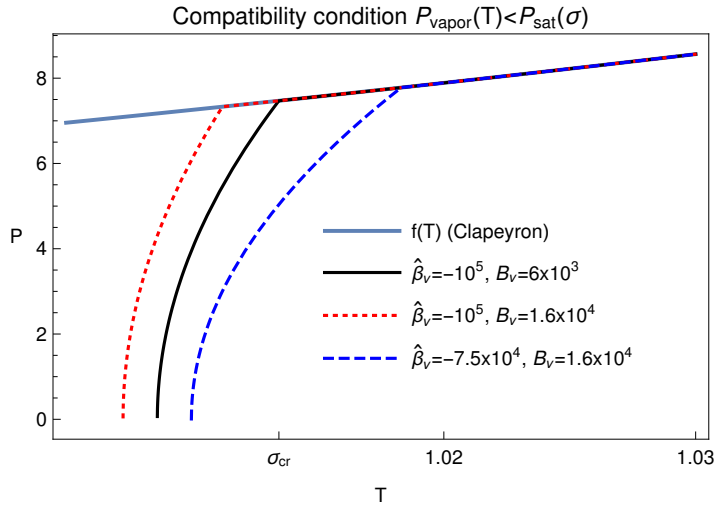


Figure 5. Check of the compatibility condition in Equation (18) for case 2.

4.3. Case 3. Recharge Due to a Single Injection Well Localized in the Liquid Domain

In this case, $\beta_v = 0$ and $d_{\ell,\text{met}} = 0$, so that Equation (26) can be rewritten as

$$D_\ell = \frac{d_{\ell,\text{inj}}\ T_s}{\gamma}$$

since $\widetilde{D}_\ell = 1$, which is the injection well located in the liquid domain. The solution to (29) is given by Equation (39), and so F as defined by Equation (33) becomes

$$\begin{aligned} F(\sigma) &= \left(\frac{d_{\ell,\text{inj}}\ T_s}{\gamma}\right)\ \left[1+\left(\frac{P_s}{rT_s\rho_{\ell,o}}\right)h(\sigma)\right] \\ &+ \left(\frac{\kappa_o P_s^2\ \gamma}{\phi_o\ r\rho_{\ell,o}\mu_o\ T_s^2}\right)\ \frac{\kappa(\sigma)\ h(\sigma)}{\phi(\sigma)\ \mu\left(f\left(\widetilde{\sigma}\right),\widetilde{\sigma}\right)}\Omega_1(\sigma) \end{aligned}$$

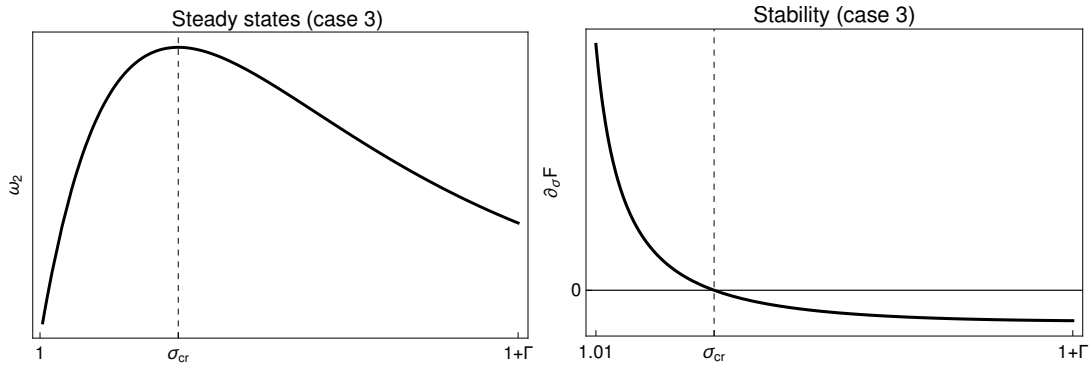
with $\Omega_1(\sigma)$ given by Equation (42). Thus, setting

$$\omega_3 = \frac{\kappa_o P_s^2\ \gamma^2}{\phi_o\ r\rho_{\ell,o}\mu_o\ T_s^3 d_{\ell,\text{inj}}},$$

the function F acquires this form:

$$F(\sigma) = 1+\omega_1\frac{f(\sigma)}{\sigma}+\omega_3\ \frac{f(\sigma)}{\sigma}\Omega_1(\sigma)\ , \tag{55}$$

where ω_1 has been defined in Equation (45), 1 without any constraints on ω_3 since Ω_1 is always strictly negative. Figure 6 shows the stable steady states in the present case and Figure 7 shows that the compatibility condition (18) is fulfilled.



(**a**) Localized liquid injection. (**b**) Stability interval.

Figure 6. (**a**) Steady statein the case of a single injection well in the liquid domain. (**b**) The critical value of σ is ≈1.053 and $\omega_{3,cr} \approx 3.3 \times 10^{-4}$. All steady states with $\sigma \in (\sigma_{cr}, 1+\Gamma)$ and $\omega_3 < \omega_{3,cr}$ are stable. In dimensional variables, the interface is located at −1723 m.

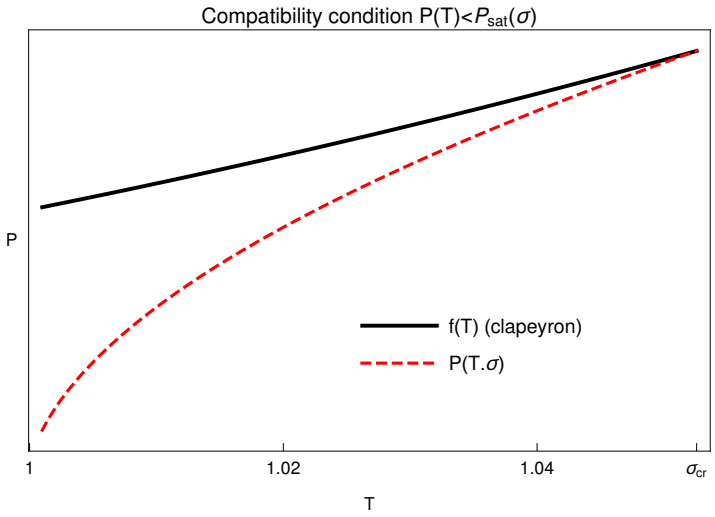


Figure 7. Check of the compatibility condition in Equation (18) for case 3.

5. Sustainability of Equilibria and Re-Injection

The main environmental and industrial issue concerning a geothermal field is the long-term sustainability of its power production capability. Since the middle of the last century, this question has been deeply discussed in the specialized literature [40,45,47,49,50], and the primary role of re-injection has been clearly emphasized. It is interesting to express the equilibrium conditions investigated in this study in dimensional variables and to compare them with some historical field data referring to the Larderello reservoir. Due to the severe approximations considered, such a comparison does not have any specific intention but to meet, at least, the order of magnitude of the most significant and available data.

An estimate of the volume V_{field} of the Larderello reservoir [10,11,14] is about 8×10^{11} m^3. Assuming the porosity of Table 1, the volume V_{fluid} of fluid in the reservoir is on the order of 1.6×10^{10} m^3. The meteoric recharge from the shallow aquifer surrounding the reservoir is not constant in time; it depends on a variety of factors and can only be roughly estimated [40]. The rate of steam extraction Q_{extr} has changed considerably during the last decades; for example, it was about 300 kg/s in the 1950s and declined to about 150 kg/s in the 1980s [11]. Precise historical series are available from ENEL, the company holding the rights of exploitation of the Larderello geothermal fields [2]. In the 1990s, the natural recharge Q_{nat} from the shallow aquifers in the area was estimated to be about one quarter of the extraction rate Q_{extr} [40]. Due to re-injection, it is likely that the ratio of

extraction/natural recharge has not changed very much [10,13]. To solve these ürpnöe,s, we assume $Q_{\text{nat}} = 0.25\, Q_{\text{extr}}$ at any time. Then, we define

$$Q_{\text{field}}(t) = -Q_{\text{extr}}(t) + Q_{\text{nat}}(t) = -0.75\, Q_{\text{extr}}(t) \tag{56}$$

Consider, now, "case 2" as discussed in Section 4.2. According to the model, the total discharge per unit volume (that is, in kg/(m^{3}s)) is given by

$$q_{\text{model}} = \rho_\ell d_{\ell,\text{met}} + d_{v,\text{met}} + d_{v,\text{inj}}, \tag{57}$$

where $d_{\ell,\text{met}}$, $d_{v,\text{met}}$ and $d_{v,\text{inj}}$ are determined by the dimensionless parameters ω_2, $\hat{\beta}_v$, and B_v through (45), 2, (46), 2, and (53), 2, i.e.,

$$d_{\ell,\text{met}} = C_1 \omega_2^{-1}, \quad d_{v,\text{met}} = C_2 B_v, \quad d_{v,\text{inj}} = C_2 \hat{\beta}_v, \tag{58}$$

where, by using data from Table 1,

$$C_1 = \frac{\kappa_o P_s^2 \gamma^2}{\phi_o r \rho_\ell \mu_o T_s^3} \approx 2.6 \times 10^{-13}\ \text{s}^{-1}, \qquad C_2 = \rho_\ell C_1 \approx 2.1 \times 10^{-10}\ \text{kg m}^{-3}\text{s}^{-1}. \tag{59}$$

For fixed values of $\hat{\beta}_v < 0$ and $B_v > 0$, any stable steady state is represented by a point (σ, ω_2), with $0 < \omega_2 < \omega_{\text{crit}}$ and $\sigma > \sigma_{\text{crit}}$, on the curve $\omega_2 = \mathfrak{F}(\sigma; \hat{\beta}_v, B_v)$. Therefore the real location of the interface depends upon the effective value of ω_2. At any time during the evolution of the reservoir, we can relate q_{model} with Q_{field} since

$$Q_{\text{field}} = q_{\text{model}} \times V_{\text{fluid}}, \tag{60}$$

and exploiting (57) and (58), we have

$$\frac{Q_{\text{field}}}{C_2 V_{\text{fluid}}} = \mathfrak{F}^{-1}(\sigma; \hat{\beta}_v, B_v) + \hat{\beta}_v + B, \tag{61}$$

where C_2 is given by Equation (59). To evaluate the left-hand side of Equation (61), we extracted some data from the historical series reported by Pallotta [2]. Notice that

$$\frac{Q_{\text{field}}}{V_{\text{fluid}}} \approx -10^{-8}\ \text{kg}/(\text{m}^3\text{s}),$$

so that $Q_{\text{field}}/\left(C_2 V_{\text{fluid}}\right) = \mathcal{O}(10^2)$ (see Table 2). Using B_v and $\hat{\beta}_v$ as free parameters, Equation (61) and Table 2 provide a simple criterion to relate the Larderello field data with the equilibrium interface. For example, selecting $Q_{\text{field}}/\left(C_2 V_{\text{fluid}}\right) = -69$ (the 2015 datum), $\hat{\beta}_v = -7.5 \times 10^4$, $B_v = 1.6 \times 10^4$, Equation (61) is fulfilled with $\sigma \approx 1.088$, (i.e., $s \approx -2220$ m), which is stable because, in case 2, with this choice of parameters, all interfaces $\sigma > 1.018$ are stable (see Figure 4). If we keep $B_v = 1.6 \times 10^4$ and decrease $\hat{\beta}_v$ up to -1.2×10^5, the new stable position of the interface is around -2560 m. According to Figures 22 and 23 in [10], at a depth of about -2000 m, the fluid pressure in 2010 was 10 bar and the temperature was around 550 K. The real fluid present in the reservoir is not pure water but a complex mixture of water, carbon dioxide and several other chemical components with a great variability of molar fractions. Even for a simple binary water–carbon dioxide system, the estimated saturation pressure would be greatly above the values reported in [10]. It must be emphasized, however, that for a real geothermal fluid, precise indications about the vapor saturation pressure are still lacking, and only some models are supplied [51–53]. This suggests, in any event, that for the Larderello field, the vapor/liquid interface must be deeper than -2000 m a.s.l. [30]. All this considered, our model, besides its indisputable simplicity and considerable approximations, locates the interface below the

above limit provided that the parameters are selected consistently with the field data. This is certainly a very encouraging result. Nomenclature and other symbol definitions can be found in Table 3.

Table 2. Production history of the Larderello field from 1960 to 2015. Artificial re-injection started in 1975.

Year	Q_{extr} (kg/s)	$Q_{\text{field}}/(C_2 V_{\text{fluid}})$
1960	412	−92
1970	287	−64
1975	241	−54
1985	255	−57
1995	266	−59
2000	275	−62
2010	294	−66
2015	315	−69

Table 3. Nomenclature and other symbol definitions.

Symbol	Description	Units	First Used in Formula
L	Reservoir thickness	m	(2)
v	Vapor velocity	$\mathrm{m\,s^{-1}}$	(3)
v_ℓ	Liquid velocity	$\mathrm{m\,s^{-1}}$	(8)
d_v	Vapor density rate	$\mathrm{kg\,m^{-3}s^{-1}}$	(4)
d_ℓ	Liquid water source density rate	$\mathrm{s^{-1}}$	(8)
δ	Dirac delta	-	(4)
D_ℓ	Total liquid recharge rate	$\mathrm{m\,s^{-1}}$	(12)
P^*	Clapeyron pressure	Pa	(15)
β_v	Pressure source term	-	(30)
Q_{field}	Reservoir flow rate	$\mathrm{kg\,s^{-1}}$	(56)
q_{mod}	Total discharge per unit volume	$\mathrm{kg\,m^{-3}s^{-1}}$	(57)
σ	Liquid/vapor interface	-	(22)
N	Number of injection heads	-	(4)
P_{inj}	Re-injection pressure	Pa	(4)
$d^{(i)}_{\ell,\text{inj}}$	i-th re-injection rate order of magnitude	$\mathrm{m\,s^{-1}}$	(13)
$\mathfrak{R}^{(i)}_\ell$	i-th liquid injection to meteoric rate ratio	-	(28)
$\mathfrak{R}^{(i)}_v$	i-th vapor injection to meteoric rate ratio	-	(31)
V_{field}	Reservoir volume	$\mathrm{m^3}$	(60)
T_o	Injection well depth	-	(47)

6. Conclusions

The main conclusion of our investigation is that stable stationary states of the liquid/vapor interface are possible either with liquid or vapor recharge combined with vapor extraction. The main parameters ω_2 (natural liquid recharge), $\beta_v < 0$ (vapor extraction) and $B_v > 0$ (vapor meteoric recharge) need to be combined conveniently to maintain a stable interface. Increasing the vapor extraction moves the interface towards the bottom of the reservoir, which at the limit is shown to be increasingly vapor-dominated. Interestingly, stable interfaces can generally be obtained only if ω_2 is less than a critical value; that is, only if the natural liquid recharge is sufficiently large.

The results obtained considering uniform porosity and permeability provide a good qualitative description of the possible steady configurations of a vapor-dominated basin such as Larderello.

An important characteristic of the model is that stationary stable states are compatible with the presence of natural and artificial recharging mechanisms. Such a conclusion agrees with the results of other geological studies [18], despite the drastic simplifications introduced in our model: 1D geometry, an absence of chemicals dissolved in water and uniform geological parameters (which, in a real geothermal field, are far from being homogeneous and may change significantly due to local

temperature and pressure). The differential Equation (19), 4, has been proven to be quite satisfactory for modeling the vapor drawdown from a reservoir and for recharging from both aquifers and injection wells. We also think that our analysis is likely to produce physically meaningful results also for equilibrium configurations of water-dominated fields. In conclusion, we believe that, despite the many simplifications made in the model, this study can be an useful step towards improving our understanding of the dynamics of geothermal fields.

Author Contributions: A.F. (Angiolo Farina), A.F. (Antonio Fasano), M.P. and F.R. have equally contributed to the conceptualization, methodology, formal analysis, writing and reviewing of the original draft of the present work. All authors have read and agreed to the submitted version of the manuscript.

Funding: This research received no external funding.

Acknowledgments: The authors wish to thank the unknown reviewers for some useful suggestions to improve the present contribution.

Conflicts of Interest: The authors declare no conflict of interest.

References

1. Manzella, A.; Serra, D.; Cesari, G.; Bargiacchi, E.; Cei, M.; Cerutti, P.; Conti, P.; Giudetti, G.; Lupi, M.; Vaccaro, M. Geothermal Energy Use, Country Update for Italy. In Proceedings of the European Geothermal Congress, The Hague, The Netherlands, 11–14 June 2019.
2. Pallotta, D. *Industrial Strategy to Contrast the Decline and Develop the Larderello System*; Technical Report; ENEL Green Power: Pisa, Italy, 2019.
3. Meacci, L.; Farina, A.; Primicerio, M. A free boundary model for the evolution of a geothermal system. *Rend. Lincei Mat. Appl.* **2019**, *30*, 125–136. [CrossRef]
4. Meacci, L.; Farina, A.; Rosso, F.; Borsi, I.; Ceseri, M.; Speranza, A. Proceedings of the Comsol Conference, Milan, Italy, 16 October 2009.Available online: https://www.comsol.com/paper/download/45984/Meacci.pdf (accessed on 15 March 2012).
5. Fasano, A.; Cerminara, M. Modelling the dynamics of a geothermal reservoir fed by gravity driven flow through overstanding saturated rocks. *J. Volcanol. Geotherm. Res.* **2012**, *233–234*, 37–54.
6. Truesdell, A.H.; White, D.E. Production of superheated steam from vapor-dominated geothermal reservoirs. *Geothermics* **1973**, *2*, 154–173. [CrossRef]
7. Nathenson, M. *Some Reservoir Engineering Calculations for the Vapor-Dominated System at Larderello, Italy*; Technical Report 75-142; U.S. Geological Survey: Menlo Park, CA, USA, 1975.
8. Pruess, K.; Narasimhan, T.N. On fluid reserves and the production of superheated steam from fractured, *vapor-dominated* geothermal reservoirs. *J. Geophys. Res. Solid Earth* **1982**, *87.B11*, 9329–9339. [CrossRef]
9. Barelli, A.; Ceiand, M.; Lovari, F.; Romagnoli, P. Numerical modeling for the Larderello-Travale geothermal system, Italy. In Proceedings of the World Geothermal Congress, Bali, Indonesia, 25–29 April 2010.
10. Romagnoli, P.; Arias, A.; Barelli, A.; Cei, M.; Casini, M. An updated numerical model of the Larderello-Travale geothermal system, Italy. *Geothermics* **2010**, *39*, 292–313. [CrossRef]
11. Cappetti, G.; Parisi, L.; Ridolfi, A.; Stefani, G. Fifteen years of reinjection in the Larderello-Valle Secolo area: analysis of the production data. In Proceedings of the World Geothermal Congress, Florence, Italy, 18–31 May 1995; pp. 1997–2000.
12. White, D.E. Characteristics of geothermal resources. In *Geothermal Energy*; Kruger, P., Otte, C., Eds.; Stanford University Press: Stanford, CA, USA, 1973; pp. 69–94.
13. Arias, A.; Dini, I.; Casini, M.; Fiordelisi, A.; Perticone, I.; Dell'Aiuto, P. Geoscientific Feature Update of the Larderello-Travale Geothermal System (Italy) for a Regional Numerical Modeling. In Proceedings of the World Geothermal Congress, Bali, Indonesia, 25–29 April 2010.
14. Ebigbo, A.; Niederau, J.; Marquart, G.; Dini, I.; Thorwart, M.; Rabbel, W.; Pechnig, R.; Bertani, R.; Clauser, C. Influence of depth, temperature, and structure of a crustal heat source on the geothermal reservoirs of Tuscany: Numerical modelling and sensitivity study. *Geotherm. Energy* **2016**. [CrossRef]
15. Dickson, M.; Fanelli, E.M. (Eds.) *Classification and Assessment of Geothermal Resources*; Chapter Small Geothermal Resources: A Guide to Development and Utilization; Centre on Small Energy Resources (UNITAR): New York, NY, USA, 1990; p. 3157.

16. Dickson, M.H.; Fanelli, M. *What Is Geothermal Energy*; Technical Report; International Institute for Geothermal Research: Pisa, Italy, 2001.
17. Bromley, C.; Mongillo, M.; Rybach, L. Sustainable utilization strategies and promotion of beneficial environmental effects. In Proceedings of the New Zealand Geothermal Workshop, Auckland, New Zealand, 15–17 November 2006.
18. Ofwona, C.O. A Reservoir Study of Olkaria East Geothermal System, Kenya. Master's Thesis, United Nations University, Geothermal Training Programme, Reykjavík, Iceland, 2002.
19. Axelsson, G.; Bromley, C.; Mongillo, M.; Rybach, L. The sustainability task of the International Energy Agency's Geothermal Implementing Agreement. In Proceedings of the World Geothermal Congress, Bali, Indonesia, 25–29 April 2010.
20. Axelsson, G.; Guðmundsson, A.; Steingrímsson, B.; Palmason, G.; Armansson, H.; Tulinius, O. Sustainable production of geothermal energy: Suggested definition. *IGA News* **2001**, *43*, 1–2.
21. Cataldi, R. Sustainability and renewability of geothermal energy. In Proceedings of the International Scientific Conference on Geothermal Energy in Underground Mines, Ustron, Poland, 21–23 November 2001; 4p.
22. O'Sullivan, M.; Yeh, A.; Mannington, W. Renewability of geothermal resources. *Geothermics* **2010**, *39*, 314–320. [CrossRef]
23. Bjarnadóttir, R. Sustainability Evaluation of Geothermal Systems in Iceland Indicators for Sustainable Production. Master's Thesis, Faculty of Mechanical and Industrial Engineering University of Iceland, Reykjavík, Iceland, 2010.
24. Axelsson, G. Using long case histories to study hydrothermal renewability and sustainable utilization. *Geotherm. Resour. Counc. Trans.* **2011**, *35*, 1393–1400.
25. Axelsson, G.; Stefánsson, V.; Björnsson, G.; Liu, J. Sustainable utilization of geothermal resources for 100–300 years. In Proceedings of the World Geothermal Congress, Antalya, Turkey, 24–29 April 2005; 8p.
26. Axelsson, G.; Björnsson, G.; Quijano, J. Reliability of lumped parameter modelling of pressure changes in geothermal reservoirs. In Proceedings of the World Geothermal Congress, Antalya, Turkey, 24–29 April 2005; 8p.
27. Axelsson, G. Sustainable geothermal utilization—Case histories, definitions, research issues and modelling. *Geothermics* **2010**, *39*, 283–291. [CrossRef]
28. Axelsson, G. Sustainable geothermal utilization. In Proceedings of the Short Course on Geothermal Development and Geothermal Wells, Santa Tecla, El Salvador, 11–17 March 2012.
29. Axelsson, G. Sustainable management of geothermal resources. In Proceedings of the SDG Short Course I on Sustainability and Environmental Management of Geothermal Resource Utilization and the Role of Geothermal in Combating Climate Change, Santa Tecla, El Salvador, 4–10 September 2016.
30. Sestini, G. Superheating of geothermal steam. *Geothermics* **1970**, *2*, 622–648. [CrossRef]
31. Celati, R.; Squarci, P.; Stefani, G.C.; Taffi, L. Study of water levels in Larderello region geothermal wells for reconstruction of reservoir pressure trend. *Geothermics* **1977**, *6*, 183–198. [CrossRef]
32. Gola, G.; Bertini, G.; Bonini, M.; Botteghi, S.; Brogi, A.; De Franco, A.; Dini, A.; Donato, A.; Gianelli, G.; Liotta, D.; et al. Data integration and conceptual modelling of the Larderello geothermal area, Italy. *Energy Procedia* **2017**, *125*, 300–309. [CrossRef]
33. Cappetti, G.; Fiordelisi, A.; Casini, M.; Ciuffi, S.; Mazzotti, A. A New Deep Exploration Program and Preliminary Results of a 3D Seismic Survey in the Larderello-Travale Geothermal Field (Italy). In Proceedings of the World Geothermal Congress, Antalya, Turkey, 24–29 April 2005; pp. 1–9.
34. Kaya, E.; O'Sullivan, M. Modelling of Injection into Vapour-Dominated Geothermal Systems. In Proceedings of the World Geothermal Congress, Bali, Indonesia, 25–29 April 2010.
35. Duffield, W.A.; Sass, J.H. *Geothermal Energy-Clean Power From the Earth's Heat*; Technical Report C1249; U.S. Department of the Interior U.S. Geological Survey: Reston, VA, USA, 2003.
36. Vasey, D.E.; Fredericks, S.E.; Shen, L.; Thompson, S. *Natural Resources and Sustainability*; Berkshire Publishing Group: Great Barrington, MA, USA, 2011.
37. Barbier, E.; Bellani, S.; Musmeci, F. The Italian geothermal database. In Proceedings of the World Geothermal Congress, Kyushu-Tohoku, Japan, 28 May–10 June 2000; pp. 3991–3995.
38. Bellani, S.; Brogi, A.; Lazzarotto, A.; Liotta, D.; Ranalli, G. Heat flow, deep temperatures and extensional structures in the Larderello Geothermal Field (Italy): constraints on geothermal fluid flow. *J. Volcanol. Geotherm. Res.* **2004**, *132*, 15–29. [CrossRef]

39. Bellani, S.; Gherardi, F. Thermal Conductivity Characterization of Larderello and Mt. Amiata Geothermal Fields. *GRC Trans.* **2013**, *37*, 231–235.
40. Celati, R.; Cappetti, G.; Calore, C.; Grassi, S.; D'Amore, F. Water recharge in Larderello geothermal field. *Geothermics* **1991**, *20*, 119–133. [CrossRef]
41. Farina, A.; Fusi, L.; Rosso, F. Mathematical models for fluids with pressure-dependent viscosity flowing in porous media. *Int. J. Eng. Sci.* **2015**, *87*, 110–118.
42. Coirier, J. *Mécanique des Milieux Continus*; Dunod: Paris, France, 1997.
43. Fasano, A.; Primicerio, M. Liquid flow in partially saturated porous media. *J. Inst. Math. Appl.* **1979**, *23*, 503–517. [CrossRef]
44. Fasano, A.; Primicerio, M. Free boundary problems for nonlinear parabolic equations with nonlinear free boundary conditions. *J. Math. Anal. Appl.* **1979**, *72*, 247–273. [CrossRef]
45. Minissale, A. The Larderello geothermal field. *Earth-Sci. Rev.* **1991**, *31*, 133–151. [CrossRef]
46. Gudmundur, S.B.; Valgardur, S. Reinjection into geothermal reservoirs. In *Geothermal Reservoir Engineering*; Okandan, E., Ed.; NATO ASI Series; Kluwer Academic Publishers: Dordrecht, The Netherland, 1988; pp. 103–120.
47. Calore, C.; Pruess, K.; Celati, R. Modeling studies of cold water injection into fluid-depleted vapor-dominated geothermal reservoirs. In Proceedings of the 11th Workshop on Geothermal Reservoir Engineering, Stanford, CA, USA, 21–23 January 1986; pp. 161–168.
48. Neri, G. Production, reinjection and well-testing in the Larderello geothermal field. In *Geothermal Reservoir Engineering*; Okandan, E., Ed.; NATO ASI Serie; Kluwer Academic Publishers: Dordrecht, The Netherland, 1988; pp. 223–240.
49. Bodvarsson, S.; Stefánsson, V. Some Theoretical and Field Aspects of Reinjection in Geothermal Reservoirs. *Water Resour. Res.* **1989**, *25*, 1235–1248. [CrossRef]
50. Stefánsson, V. Geothermal Reinjection Experience. *Geothermics* **1997**, *26*, 99–139. [CrossRef]
51. Spycher, N.; Pruess, K. A Phase-Partitioning Model for CO_2–Brine Mixtures at Elevated Temperatures and Pressures: Application to CO_2-Enhanced Geothermal Systems. *Transp. Porous Media* **2010**, *82*, 173–196. [CrossRef]
52. Pruess, K. *Mathematical Modeling of Fluid Flow and Heat Transfer in Geothermal Systems—An Introduction in Five Lectures*; Technical Report 3; The United Nations University, Geothermal Training Programme, Orkustofnun, Grensásvegur 9: Reykjavík, Iceland, 2002.
53. Efika, E.C.; Hoballah, R.; Li, X.; May, E.F.; Nania, M.; Sanchez-Vicente, Y.; Trusler, J.M. Saturated phase densities of (CO_2+H_2O) at temperatures from (293 to 450)K and pressures up to 64MPa. *J. Chem. Thermodyn.* **2016**, *93*, 347–359. [CrossRef]

Publisher's Note: MDPI stays neutral with regard to jurisdictional claims in published maps and institutional affiliations.

© 2020 by the authors. Licensee MDPI, Basel, Switzerland. This article is an open access article distributed under the terms and conditions of the Creative Commons Attribution (CC BY) license (http://creativecommons.org/licenses/by/4.0/).